energies

MDPI

Article

High Breakdown Field $CaCu_3Ti_4O_{12}$ Ceramics: Roles of the Secondary Phase and of Sr Doping

Zhuang Tang, Kangning Wu, Yuwei Huang and Jianying Li *

State Key Laboratory of Electrical Insulation and Power Equipment, Xi'an Jiaotong University, Xi'an 710049, China; frank11.25@stu.xjtu.edu.cn (Z.T.); Wukangning666@stu.xjtu.edu.cn (K.W.); i10035004@stu.xjtu.edu.cn (Y.H.)

* Correspondence: lijy@mail.xjtu.edu.cn; Tel.: +86-29-8266-5703

Academic Editor: Issouf Fofana

Received: 30 March 2017; Accepted: 16 May 2017; Published: 19 July 2017

Abstract: In this work, two methods of $CaCu_3Ti_4O_{12}$-$CuAl_2O_4$ composite and $SrCu_3Ti_4O_{12}$-$CaCu_3Ti_4O_{12}$ composite were prepared to improve the breakdown field in $CaCu_3Ti_4O_{12}$ ceramics. $CaCu_3Ti_4O_{12}$-$0.5CuAl_2O_4$ and $0.4SrCu_3Ti_4O_{12}$-$0.6CaCu_3Ti_4O_{12}$ samples with proper sintering conditions were found to have greatly enhanced breakdown fields of more than 20 $kV{\cdot}cm^{-1}$ compared to the ordinary value of 1–2 $kV{\cdot}cm^{-1}$ in $CaCu_3Ti_4O_{12}$ ceramics. In addition, reduced dielectric loss tangent of these samples remained about 0.1 at a low frequency of 0.1 Hz, indicating superior dielectric properties. No abnormal grain growth was found in either composite with a high breakdown field, which was attributed to the pining effect and consumption of Cu-rich phase at grain boundaries. Under analysis of the relaxation process by electric modulus, compared to conventional $CaCu_3Ti_4O_{12}$ ceramics, interstitial $Al_i^{\cdots}$ and increasing interfaces were responsible for variation in activation energy in $CaCu_3Ti_4O_{12}$-$0.5CuAl_2O_4$ composites, while the integrated action of a strong solid solution effect and weak Sr-stretching effect contributed to the elevated potential barrier height and enhanced breakdown field in $0.4SrCu_3Ti_4O_{12}$-$0.6CaCu_3Ti_4O_{12}$ composites.

Keywords: CCTO-based ceramics; breakdown field; pining effect; oxygen vacancy

1. Introduction

$CaCu_3Ti_4O_{12}$ (CCTO) ceramics has been extensively studied due to its colossal dielectric constant (CDC) up to 10^5, which is frequency independent in 10^2–10^6 Hz and exhibits excellent temperature stability over 100–600 K [1]. In addition to CDC, non-ohmic characteristic has also been found in CCTO ceramics [2], which is promising in applications of energy storage capacitors and over-voltage protection devices. Both the CDC property and non-ohmic characteristics are associated with defect-related double Schottky barrier between the semiconducting grains and insulating grain boundaries [3–5]. The Schottky barrier blocks charge transport at grain boundaries, resulting in high nonlinear coefficient [2] and active dipole movement for CDC property in an internal barrier layer capacitor (IBLC) model [6].

It has been accepted that electrical property of CCTO ceramics is sensitive to the preparing method and the material composition [7,8]. Particularly, changes in the compositions to fabricate CCTO-based composite ceramics can notably affect the grain boundary structure and thus the dielectric performance [9,10]. In situ synthesis is an effective way to introduce homogeneous distribution of secondary phase. The phase equilibrium relations in the $Cu_2O/CuO/Al_2O_3$ [11] system showed that, above 900 °C, the spinel phase of $CuAl_2O_4$ can be easily synthesized. Since the sintering temperature of CCTO ceramics is generally higher than 1000 °C, it can be expected that the spinel phase of $CuAl_2O_4$, which is unlike the perovskite-like phase in previously reported literature, can be easily synthesized in situ via the addition of Al_2O_3. The spinel phase is generally of high resistance, and the consumption

of Cu-rich liquid phase by $CuAl_2O_4$ can help to control the grain growth. Meanwhile, composite ceramics with CCTO and other materials are also studied to improve the non-ohmic properties. A composite system of CCTO/$CaTiO_3$ (CCTO/CTO) has been reported by Kobayashi and Terasaki to have achieved a greatly reduced tan δ as well as an enhanced nonlinear coefficient and a breakdown electric field [10,12]. CCTO/$Y_{2/3}Cu_3Ti_4O_{12}$ composite ceramics have been developed as increased nonlinear coefficients with low dielectric loss, obtained [13] in our previous work.

In most research, the majority of breakdown fields for CCTO ceramics are less than 2 kV·cm^{-1} [14,15]. According to the formula of stored energy $U = (\varepsilon' {E_b}^2)/2$, breakdown fields strongly affect the maximum stored energy. In our previous work, the breakdown voltage of CCTO could be enhanced to 13 kV·cm^{-1} with a dielectric constant of more than 1000 by direct introduction of secondary $CuAl_2O_4$ phase [16]. The improvement of the breakdown field is focused in this work by two different methods: $CaCu_3Ti_4O_{12}$-$CuAl_2O_4$ composite ceramics by in situ synthesis and $SrCu_3Ti_4O_{12}$-$CaCu_3Ti_4O_{12}$ composite ceramics, respectively. Phase composition, microstructure, nonlinearity, and breakdown fields are investigated in this work. In addition, based on the analysis of the dielectric relaxation process, the reasons for the enhanced breakdown fields are discussed related to the potential barrier at the grain boundary.

2. Materials and Methods

The $0.4SrCu_3Ti_4O_{12}$-$0.6CaCu_3Ti_4O_{12}$ ceramics were prepared through a conventional solid-state reaction method with the raw material of high-purity (>99%) $SrCO_3$, $CaCO_3$, CuO, and TiO_2. Initially, powders of $SrCu_3Ti_4O_{12}$ and $CaCu_3Ti_4O_{12}$ were separately prepared. Stoichiometric amounts of these raw materials were mixed by ball milling in ethanol for 8 h. The dried mixture powders were calcined in air at 950 °C for 15 h. Then, the calcined powders including both $SrCu_3Ti_4O_{12}$ and $CaCu_3Ti_4O_{12}$ were mixed together according to an Sr/Ca ratio of 4:6. Mixed powders were ground in ethanol for 8 h and sieved, and 3 wt % polyvinyl alcohol was added as a binder. Next, the presintered powders were pressed to green pellets with a 12 mm diameter and a 1.2 mm thickness under 100 MPa. Finally, the pellets were sintered in air at 1000 °C for 5 h and 15 h, respectively, and furnace cooled to room temperature.

For in situ $CuAl_2O_4$ phase in CCTO ceramics, CCTO powder was prepared through a solid-state reaction method. After CCTO powder was suspended in an $Al(NO_3)_3$ aqueous solution, the suspension was quantitatively titrated with NH_4OH to obtain $Al(OH)_3$ precipitation on the surface of CCTO particles. The obtained powder was dried and calcined at 950 °C for 4 h to dehydrate $Al(OH)_3$ into Al_2O_3. Then, powder was pressed into pellets with a diameter of 12 mm and a thickness of 1.6 mm. Finally, presintered powder was sintered in air at 1100 °C for 4 h. The corresponding chemical reactions are as follows:

$$2Al(OH)_3 = Al_2O_3 + 3H_2O \uparrow \quad (1)$$

$$CuO + Al_2O_3 = CuAl_2O_4 \quad (2)$$

$$Cu_2O + 2Al_2O_3 + \frac{1}{2}O_2 = 2CuAl_2O_4. \quad (3)$$

Phase compositions of sintered ceramics were characterized by X-ray diffraction (XRD, Regaku D/MAX IIIB, Regaku, Tokyo, Japan) in a 2θ scanning from 15 to 80°. Microstructures and element distributions of the samples were examined by field emission scanning electron microscopy (FESEM, JEOL JSM-7800F, JEOL, Tokyo, Japan). For measurement of electrical properties, both sides of sintered samples were polished and sputtered with gold (KYKY SBC-128, KYKY Technology, Beijing, China). *I-V* behavior was measured by HP 34401A multimeter with a WJ10001D precision linear high-voltage direct current (dc) power. Measurement of dielectric performance was carried out by broadband dielectric spectrometer (Concept 80, Novocontrol Technologies, Montabaur, Germany) in frequency range of 10^{-1}–10^7 Hz.

3. Results and Discussion

XRD patterns of undoped CCTO ceramics, $CaCu_3Ti_4O_{12}$-$0.5CuAl_2O_4$ composite and $0.4CaCu_3Ti_4O_{12}$-$0.6CaCu_3Ti_4O_{12}$ composite is shown in Figure 1. Obviously, all of the samples exhibit one main perovskite phase, which is cubic perovskite-related-structure (space group Im3) CCTO, by comparison with the standard Powder Diffraction File Database [JCPDS-05-0566 #75-2188]. Besides, the in-situ formed phase of spinel $CuAl_2O_4$ can be detected in $CaCu_3Ti_4O_{12}$-$0.5CuAl_2O_4$ samples. However, in 0.4SCTO-0.6CCTO composites, no second phase is detected. Since the radius of Sr^{2+} is larger than that of Ca^{2+}, the main peak of XRD patterns moves towards lower angles in 0.4SCTO-0.6CCTO composites, which could also be verified in the inset of Figure 1.

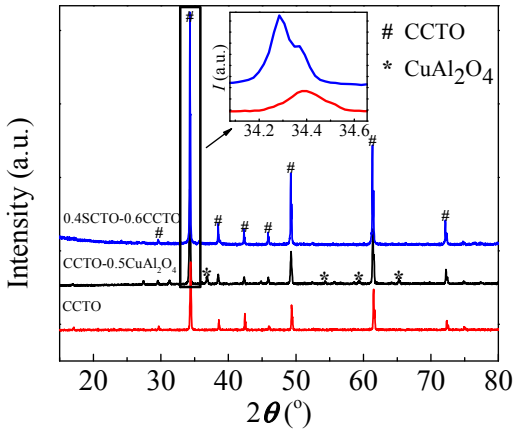

Figure 1. XRD patterns of undoped CCTO ceramics, the $CaCu_3Ti_4O_{12}$-$0.5CuAl_2O_4$ composite, and the $0.4SrCu_3Ti_4O_{12}$-$0.6CaCu_3Ti_4O_{12}$ composite. Inset is the magnification of main peak for CCTO and $0.4SrCu_3Ti_4O_{12}$-$0.6CaCu_3Ti_4O_{12}$.

Microstructures of CCTO-$0.5CuAl_2O_4$ and 0.4SCTO-0.6CCTO ceramics and pure CCTO in different sintering times are given in Figure 2. For in-situ $CuAl_2O_4$ phase samples, grain size with uniform distribution ranges from 1 to 4 μm and the second phase of $CuAl_2O_4$ locates intergranularly in samples sintered for 4 h. However, abnormal growth of CCTO grains occurs in samples sintered for 20 h, which is a common phenomenon in CCTO ceramics, leading to a grain size of more than 50 μm. Meanwhile, the second phase of $CuAl_2O_4$ is partially coated by giant CCTO grains. For 0.4SCTO-0.6CCTO ceramics, no abnormal grain growth is observed in either sintering condition. Two categories of grains are found in SEM images, including cuboid grains, with a size of more than 2 μm and spherical grains with a size less than 2 μm. In the grain growth process, the second phase has a significant inhibitory effect on the migration of the grain boundary, which is called pinning effect. The effect is represented through the Zener model [17].

$$\frac{G}{r} = \frac{4}{3} f^{-1} \tag{4}$$

where G is the limit size of the matrix grain in the presence of the second phase pinning, r and f are respectively the particle diameter and the volume fraction of the second phase. It is considered that as the grain size of the second phase decreases and the volume fraction of the second phase increases, the matrix grain size apparently declines.

In this paper, for CCTO-$CuAl_2O_4$ composites sintered for 4 h, the second phase of $CuAlO_4$ is uniformly located among the CCTO grains, which can effectively consume the Cu-rich phase and obstruct the contact of CCTO grains. The pinning effect of $CuAlO_4$ affects the mass transfer process and thus impedes the abnormal grain growth of CCTO grains. For CCTO-$CuAl_2O_4$ composites sintered for 20 h, Figure 2b shows that partial $CuAlO_4$ is swallowed by the CCTO grains, leading to reduced

$CuAlO_4$ located intergranularly and a weakened pining effect. In 0.4SCTO-0.6CCTO composites, it is obvious that the grain size of 0.4SCTO-0.6CCTO composites are sharply decreased compared to pure CCTO samples in Figure 2e,f. The pining effect in 0.4SCTO-0.6CCTO is slightly different from that in CCTO-$CuAl_2O_4$ composites. No nominal second phase exists in the composites since only one main phase of CCTO is detected in XRD. However, the interfaces in 0.4SCTO-0.6CCTO composites consist of interfaces between SCTO/SCTO, SCTO/CCTO, and CCTO/CCTO, which can effectively hinder grain growth. Moreover, under the transport action of $SrTiO_3$ [18,19], partial Cu-rich phase transfers from grain boundary into grain, thus decreasing the formation of Cu-rich phase at the grain boundary and impeding abnormal grain growth.

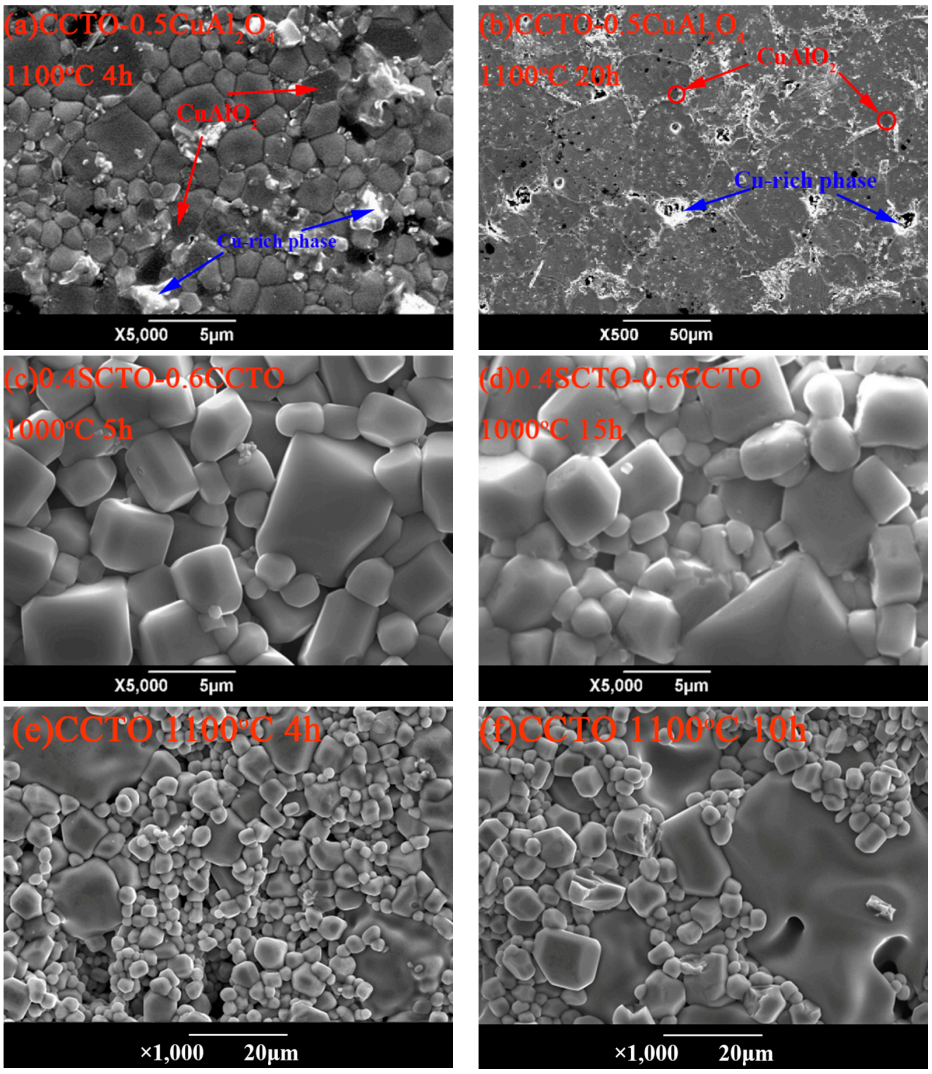

Figure 2. Microstructure of $CaCu_3Ti_4O_{12}$-0.5$CuAl_2O_4$ sintered for 4 h (**a**) and 20 h (**b**); 0.4$SrCu_3Ti_4O_{12}$-0.6$CaCu_3Ti_4O_{12}$ sintered for 5 h (**c**) and 15 h (**d**); and pure CCTO sintered for 4 h (**e**) and 10 h (**f**).

The current density (*J*)-breakdown field (*E*) characteristics of CCTO, CCTO-0.5$CuAl_2O_4$, and 0.4SCTO-0.6CCTO ceramics is given in Figure 3a. The current range is from 0.5 to 500 μA. The breakdown field is defined as the electric field when the current density is around 0.6 $mA{\cdot}cm^{-2}$. Results of the breakdown field and the nonlinear coefficient are shown in Figure 3b. It can be found that the CCTO-0.5$CuAl_2O_4$ and 0.4SCTO-0.6CCTO samples show an extremely high breakdown electric field E_b of about 20 $kV{\cdot}cm^{-1}$, which is almost 10 times of former works in both pure CCTO ceramics [3,20]

and CCTO-based composite ceramics [9]. The breakdown field of 0.4SCTO-0.6CCTO samples sintering at 1000 °C for 5 h even reaches 23.8 kV·cm^{-1} and that of CCTO-0.5$CuAl_2O_4$ samples also achieves 21 kV·cm^{-1}, which are the highest values ever reported. As the SEM images show, the pining effect of the second phase can effectively reduce the grain size, which can lead to the enhancement of the breakdown field. In addition, the consumption of Cu-rich by $CuAlO_2$ in CCTO-0.5$CuAl_2O_4$ and the transport action of $SrTiO_3$ in 0.4SCTO-0.6CCTO result in even higher E_b. The nonlinear coefficients are calculated in the current range of 50–500 μA. It is clearly shown in Figure 3b that nonlinear coefficients do not decrease with enhanced breakdown fields, maintaining excellent nonlinear properties.

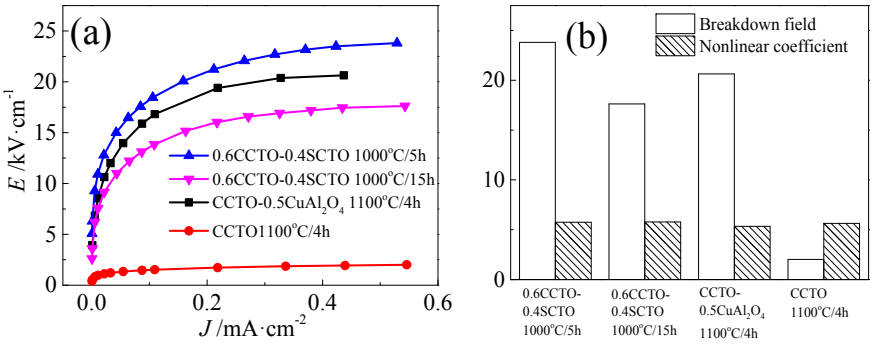

Figure 3. *J-E* plots (**a**) and breakdown field, nonlinear coefficient (**b**) of CCTO, CCTO-0.5$CuAl_2O_4$, and 0.4SCTO-0.6CCTO ceramics.

Permittivity and dielectric loss at room temperature of CCTO, CCTO-0.5$CuAl_2O_4$, and 0.4SCTO-0.6CCTO ceramics are presented in Figure 4. It can be seen that permittivity of both CCTO-0.5$CuAl_2O_4$ and 0.4SCTO-0.6CCTO ceramics are much smaller than that of pure CCTO ceramics but still reach more than 1000. Nevertheless, compared to high dielectric loss of more than 2 in CCTO ceramics at 0.1 Hz, the stable permittivity at low frequency (less than 10 Hz) in CCTO-0.5$CuAl_2O_4$ and 0.4SCTO-0.6CCTO suppress the dielectric loss effectively, resulting in the low dielectric loss of about 0.1 even at 0.1 Hz. A similar phenomenon is also observed in the CCTO/$MgTiO_3$ [9] and CCTO/$CaTiO_3$ [21] composite ceramics, and it has been attributed to the missing charge carriers. In addition, according to the formula of stored energy $U = (\varepsilon' E_b^2)/2$, the maximum U calculated for CCTO-0.5 $CuAl_2O_4$ and 0.4SCTO-0.6CCTO samples are correspondingly 44.1 and 50.9 kJ·m^{-3} in this work, which is a great improvement over that of CCTO ceramics of 2–7 kJ·m^{-3} in previous works [1,3,20,21].

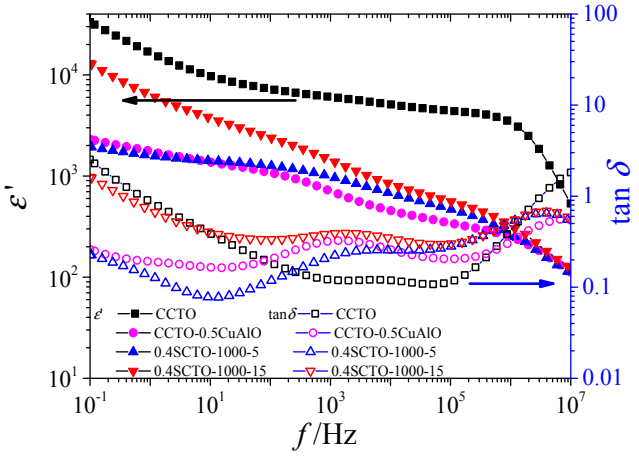

Figure 4. Dielectric performance at room temperature of CCTO, CCTO-0.5$CuAl_2O_4$, and 0.4SCTO-0.6CCTO ceramics.

The influence of $CuAl_2O_4$ and $SrCu_3Ti_4O_{12}$ on the relaxation process of CCTO was also investigated in this research. Electrical modulus is considered to be more effective in analyzing the relaxation process of polycrystalline ceramics since the large density of the mobile charge carriers is not taken into account in this formalism [22]. The electric modulus is defined as the reciprocal of complex permittivity:

$$M^* = \frac{1}{\varepsilon^*} = \frac{1}{\varepsilon' - j\varepsilon''} = \frac{\varepsilon'}{\varepsilon'^2 + \varepsilon''^2} + j\frac{\varepsilon''}{\varepsilon'^2 + \varepsilon''^2} = M' + jM'' \quad (5)$$

where $M' = \varepsilon'/(\varepsilon'^2 + \varepsilon''^2)$ and $M'' = \varepsilon''/(\varepsilon'^2 + \varepsilon''^2)$ are the real and imaginary part of complex electric modulus. Three relaxation peaks can be observed for all the samples in electric modulus plots in temperature range 153–433 K, shown in Figure 5. The peak frequencies shift to higher frequencies as temperature increases, and their corresponding activation energy levels are calculated in Figure 6, according to Arrhenius' law. Breakdown fields E_b and activation energy of relaxations are given in Table 1.

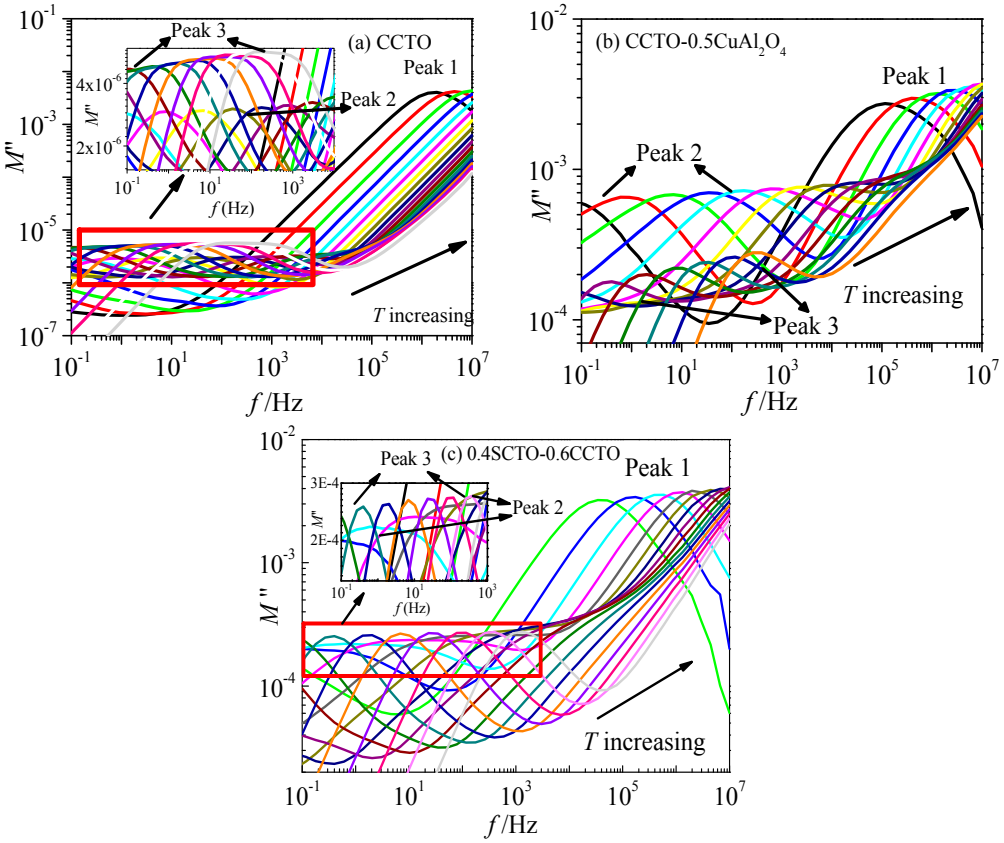

Figure 5. Frequency dependence of electric modulus in the temperature range of 153–433 K for CCTO ceramics (**a**), the $CaCu_3Ti_4O_{12}$-0.5$CuAl_2O_4$ composite (**b**), and the 0.4SCTO-0.6CCTO composite (**c**).

Table 1. Electrical parameters of CCTO ceramics of undoped CCTO ceramics and $CaCu_3Ti_4O_{12}/CuAl_2O_4$ composite ceramics.

Sample	E_b (kV·cm^{-1})	L_1 (eV)	L_2 (eV)	L_3 (eV)
undoped CCTO	2.2	0.11	0.47	0.65
$CaCu_3Ti_4O_{12}$-0.5$CuAl_2O_4$	21	0.15	0.35	0.84
0.4SCTO-0.6CCTO	23.8	0.14	0.48	0.88

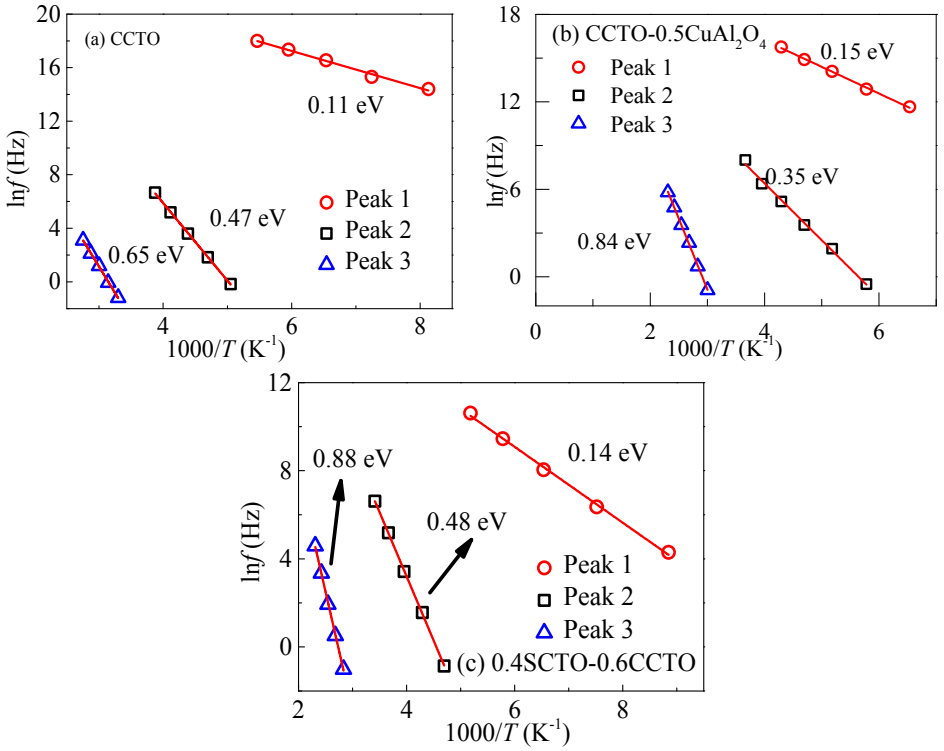

Figure 6. Frequency dependence of the electric modulus in the temperature range of 153–433 K for undoped CCTO ceramics (**a**), $CaCu_3Ti_4O_{12}/CuAl_2O_4$ composite (**b**) and 0.4SCTO-0.6CCTO (**c**).

Peak 1 in Figure 5 is commonly considered as the intrinsic bulk or grain relaxation in CCTO ceramics [6]. Activation energy of Peak 1 is 0.11 eV for CCTO ceramics, while this value is about 0.13 eV for the CCTO-0.5$CuAl_2O_4$ composite and 0.14 eV for the 0.4SCTO-0.6CCTO composite. In the CCTO-0.5$CuAl_2O_4$ composite, since the radius of Al^{3+} (0.535 Å) is close to that of Ti^{4+} (0.605 Å), Al^{3+} tends to substitute Ti^{4+} to form the Al_{Ti}'. As the grains of CCTO are n-type semiconducting, the carrier concentration will be reduced according to the substitution. Additionally, in recent work, Al^{3+} concentration is much higher than its solid solubility limit in CCTO [23]. Thus, interstitial $Al_i^{\cdots}$ can be generated from Al^{3+} filling in the gaps of unit cell, which are caused by Cu-deficiency. Therefore, charge carriers in n-type semiconducting grains are partially compensated, and defect structures can be restrained, leading to a slight increase in the intrinsic energy level. The decline of the dielectric response in Figure 4 at high frequency can also be explained by this inhibition effect. In the 0.4SCTO-0.6CCTO composites, since cation-O bonds do not need much energy [24], oxygen vacancies can be considered a reasonable source for electron formation. However, the solid solution effect of Sr^{2+} in CCTO and Ca^{2+} in SCTO has an inhibitory effect on the intrinsic oxygen vacancy defects. After Ca^{2+} or Sr^{2+} is involved in solid solution, the generation of oxygen vacancy is difficult to achieve, thus increasing the intrinsic activation energy [25].

In the single-phase CCTO ceramics, Peak 2 is derived from the intrinsic defect closely related to the oxygen vacancy, corresponding to the deep trap energy level in the depletion layer. Introduction of the interstitial $Al_i^{\cdots}$ makes the composition of the positive charge in the depletion layer more complex. Dielectric loss related with Peak 2 and relevant activation energy should reduce by interstitial $Al_i^{\cdots}$ suppressing the generation of oxygen vacancy. However, it can be seen from Figure 4 that the dielectric loss for CCTO-0.5$CuAl_2O_4$ composite at intermediate frequency is greatly strengthened compared with the CCTO sample, indicating that the relaxation mechanism corresponding to Peak 2 may not transform into the oxygen vacancy dominance. The depletion of the deep trap caused by the interstitial $Al_i^{\cdots}$ in the depletion layer may be the reason for the decrease activation energy of Peak 2.

Peak 3 in Figure 5 is supposed to be related to M–W relaxation at grain boundary, increasing apparently from 0.65 in CCTO ceramics to 0.84 and 0.88 eV in composite ceramics. The activation energy is considered closely associated with conduction process at low frequency and controlled by the potential barrier at the grain boundary. For in-situ formed $CuAl_2O_4$ samples, on one hand, the introduction of the second phase leads to a more sophisticated interface in CCTO-$CuAl_2O_4$ composites, such as the interface between CCTO/CCTO, CCTO/$CuAl_2O_4$, and $CuAl_2O_4$/$CuAl_2O_{40}$ [26], attributing to the rise of interface density. Combined with the interstitial $Al_i^{\cdots}$ suppressing on the generation of oxygen vacancy, potential barrier height is elevated in CCTO-$CuAl_2O_4$ composites. On the other hand, the potential barriers of the grain boundary for 4 h and 20 h samples are calculated as 0.81 eV and 0.74 eV, respectively, which can explain the discrepancy in the pining effect. The potential barriers for samples sintered for 4 h are larger than that of samples sintered for 20 h, indicating that the pining effect is weakened in these samples. The discrepancy in the pining effect can lead to distinct nonlinear properties.

For SCTO-CCTO composites, since the solid solution effect of Sr^{2+} in CCTO and Ca^{2+} in SCTO and has an inhibitory effect on the intrinsic oxygen vacancy defects, the donor density in 0.4SCTO-0.6CCTO is in a relatively low level. Meanwhile, potential barrier height at the grain boundary is inversely proportional to donor density, leading to the elevated potential barrier height of 0.88 eV in 0.4SCTO-0.6CCTO composites. Nevertheless, the space for the *A* site in CCTO is very rigid since the expected Ca–O distance is 2.72 Å, while the observed distance is 2.61 Å [27]. As the radius of Sr is much larger than that of Ca, Sr–O bonds are in an extremely overbonded situation. The Sr–O distance is expected to be 2.82 Å while the observed Sr–O distance is 2.64 Å [27]. When the Sr/Ca ratio is increasing on the *A* site, the larger Sr stretches the Ti–O bonds and influences the tilted TiO_6 octahedra, thus enhancing the polarizability of the tilted TiO_6 octahedra and possibly breaking the balance of Cu–O planar [28]. At this point, the generation of oxygen vacancy much more easily increases the donor density when Sr/Ca ratio increases. Only when the Sr/Ca ratio is 4:6, the integrated action of the strong solid solution effect and the weak Sr-stretching effect contributes to the elevated potential barrier height and enhanced breakdown field.

4. Conclusions

In summary, $CaCu_3Ti_4O_{12}$-0.5$CuAl_2O_4$ composites prepared by an in-situ method and 0.4$SrCu_3Ti_4O_{12}$-0.6$CaCu_3Ti_4O_{12}$ composites by a solid-state method were found to exhibit remarkably enhanced breakdown fields. In addition, permittivity still maintains more than 1000 while the dielectric loss remains about 0.1 even at a low frequency of 0.1 Hz, indicating excellent dielectric properties:

1. The breakdown field for CCTO-0.5$CuAl_2O_4$ sintering at 1100 °C for 4 h can reach 21 kV·cm^{-1}. The microstructure shows that no abnormal grain growth appears in samples with high breakdown fields, which can be attributed to the pining effect and consumption of the Cu-rich phase at the grain boundaries, contributing directly to the increase in breakdown field. Interstitial $Al_i^{\cdots}$ and increasing interfaces owing to the second $CuAl_2O_4$ phase are possible reasons for the variation in activation energy compared to the CCTO ceramics.
2. The breakdown field for 0.4SCTO-0.6CCTO sintering at 1000 °C for 5 h can even achieve 23.8 kV·cm^{-1}, which are the highest values ever reported. Under the transport action of $SrTiO_3$, some Cu-rich phase transfers from the grain boundary into the grain, decreasing the formation of Cu-rich phase at the grain boundary and impeding abnormal grain growth. Integrated action of a strong solid solution effect and a weak Sr-stretching effect contributes to the elevated potential barrier height and enhanced breakdown field.

Acknowledgments: This work is supported by the National Natural Science Foundation of China (No. 51177121) and (No. 51221005) and the Natural Science Foundation of Shaanxi Province (No. 2015JM5243).

Author Contributions: Jianying Li and Zhuang Tang conceived and designed the experiments; Yuwei Huang and Zhuang Tang performed the experiments; Kangning Wu and Zhuang Tang analyzed the data; Kangning Wu

contributed analysis tools; Zhuang Tang wrote the paper; Jianying Li and Kangning Wu offered suggestions about the paper.

Conflicts of Interest: The authors declare no conflict of interest.

References

1. Ramirez, A.P.; Subramanian, M.A.; Gardel, M.; Blumberg, G.; Li, D.; Vogt, T.; Shapiro, S.M. Giant dielectric constant response in a copper-titanate. *Solid State Commun.* **2000**, *115*, 217–220. [CrossRef]
2. Chung, S.; Kim, I.; Kang, S.L. Strong nonlinear current-voltage behaviour in perovskite-derivative calcium copper titanate. *Nat. Mater.* **2004**, *3*, 774–778. [CrossRef] [PubMed]
3. Lu, Z.; Li, X.; Wu, J. Voltage-current nonlinearity of $CaCu_3Ti_4O_{12}$ ceramics. *J. Am. Ceram. Soc.* **2012**, *95*, 476–479. [CrossRef]
4. Zang, G.; Zhang, J. Grain boundary effect on the dielectric properties of $CaCu_3Ti_4O_{12}$ ceramics. *J. Phys. D Appl. Phys.* **2005**, *38*, 1824. [CrossRef]
5. Adams, T.B.; Sinclair, D.C.; West, A.R. Characterization of grain boundary impedances in fine- and coarse-grained $CaCu_3Ti_4O_{12}$ ceramics. *Phys. Rev. B* **2006**, *73*, 94124. [CrossRef]
6. Sinclair, D.C.; Adams, T.B.; Morrison, F.D.; West, A.R. $CaCu_3Ti_4O_{12}$: One-step internal barrier layer capacitor. *Appl. Phys. Lett.* **2002**, *80*, 2153–2155. [CrossRef]
7. Fang, T.; Mei, L.; Ho, H. Effects of Cu stoichiometry on the microstructures, barrier-layer structures, electrical conduction, dielectric responses, and stability of $CaCu_3Ti_4O_{12}$. *Acta Mater.* **2006**, *54*, 2867–2875. [CrossRef]
8. Deng, G.; Muralt, P. Annealing effects on electrical properties and defects of $CaCu_3Ti_4O_{12}$ thin films deposited by pulsed laser deposition. *Phys. Rev. B* **2010**, *81*, 224111. [CrossRef]
9. Yuan, J.; Lin, Y.H.; Lu, H.; Cheng, B.; Nan, C.W. Dielectric and varistor behavior of $CaCu_3Ti_4O_{12}$-$MgTiO_3$ composite ceramics. *J. Am. Ceram. Soc.* **2011**, *94*, 1966–1969. [CrossRef]
10. Kobayashi, W.; Terasaki, I. $CaCu_3Ti_4O_{12}/CaTiO_3$ composite dielectrics: Ba/Pb-free dielectric ceramics with high dielectric constants. *Appl. Phys. Lett.* **2005**, *87*, 32902–32903. [CrossRef]
11. Jacob, K.T.; Alcock, C.B. Thermodynamics of $CuAlO_2$ and $CuAl_2O_4$ and Phase Equilibria in the System Cu_2O-CuO-Al_2O_3. *J. Am. Ceram. Soc.* **1975**, *58*, 192–195. [CrossRef]
12. Ramírez, M.A.; Bueno, P.R.; Tararam, R.; Cavalheiro, A.A.; Longo, E.; Varela, J.A. Evaluation of the Effect of the Stoichiometric Ratio of Ca/Cu on the Electrical and Microstructural Properties of the $CaCu_3Ti_4O_{12}$ Polycrystalline System. *J. Phys. D Appl. Phys.* **2009**, *42*, 185503. [CrossRef]
13. Li, J.Y.; Wu, K.N.; Jia, R.; Hou, L.L.; Gao, L.; Li, S.T. Towards Enhanced Varistor Property and Lower Dielectric Loss of $CaCu_3Ti_4O_{12}$ Based Ceramics. *Mater. Des.* **2016**, *92*, 546–551. [CrossRef]
14. Li, T.; Chen, Z.; Chang, F.; Hao, J.; Zhang, J. The effect of Eu_2O_3 doping on $CaCu_3Ti_4O_{12}$ varistor properties. *J. Alloy. Compd.* **2009**, *484*, 718–722. [CrossRef]
15. Cheng, B.; Lin, Y.H.; Deng, W.; Cai, J.N.; Lan, J.L.; Nan, C.W.; Xiao, X.; He, J.L. Dielectric and nonlinear electrical behaviors of Ce-doped $CaCu_3Ti_4O_{12}$ ceramics. *J. Electroceram.* **2012**, *29*, 250–253. [CrossRef]
16. Li, J.Y.; Hou, L.L.; Jia, R.; Gao, L.; Wu, K.N.; Li, S.T. Influences of $CuAl_2O_4$ doping on the dielectric properties of $CaCu_3Ti_4O_{12}$ ceramics. *J. Mater. Sci. Mater. Electron.* **2015**, *26*, 5085–5091. [CrossRef]
17. Zener, C.; Smith, C. Grains, phases, and interfaces: An interpretation of microstructure. *Trans. Metall. Soc. AIME* **1948**, *175*, 15–51.
18. Lu, J.; Wang, D.; Zhao, C. $CaCu_3Ti_4O_{12}$ ceramics from basic co-precipitation (BCP) method: Fabrication and properties. *J. Alloy. Compd.* **2011**, *509*, 3103–3107. [CrossRef]
19. Yan, Y.; Jin, L.; Feng, L.; Cao, G. Decrease of dielectric loss in giant dielectric constant $CaCu_3Ti_4O_{12}$ ceramics by adding $CaTiO_3$. *Mater. Sci. Eng. B* **2006**, *130*, 146–150. [CrossRef]
20. Cheng, B.; Lin, Y.H.; Yuan, J.; Cai, J.; Nan, C.W.; Xiao, X.; He, J. Dielectric and nonlinear electrical behaviors of La-doped $CaCu_3Ti_4O_{12}$ ceramics. *J. Appl. Phys.* **2009**, *106*, 34111–34114. [CrossRef]
21. Jumpatam, J.; Thongbai, P.; Kongsook, B.; Yamwong, T.; Maensiri, S. High permittivity, low dielectric loss, and high electrostatic potential barrier in $Ca_2Cu_2Ti_4O_{12}$ ceramics. *Mater. Lett.* **2012**, *76*, 40–42. [CrossRef]
22. Roling, B.; Happe, A.; Funke, K.; Ingram, M.D. Carrier concentrations and relaxation spectroscopy: New information from scaling properties of conductivity spectra in ionically conducting glasses. *Phys. Rev. Lett.* **1997**, *78*, 2160–2163. [CrossRef]

23. Choi, S.; Hong, S.; Kim, Y. Effect of Al doping on the electric and dielectric properties of $CaCu_3Ti_4O_{12}$. *J. Am. Ceram. Soc.* **2007**, *90*, 4009–4011. [CrossRef]
24. Matos, M.; Walmsley, L. Cation–oxygen interaction and oxygen stability in $CaCu_3Ti_4O_{12}$ and $CdCu_3Ti_4O_{12}$ lattices. *J. Phys. Condens. Matter* **2006**, *18*, 1793–1803. [CrossRef]
25. Kim, S.; Jung, W.H.; Inaguma, Y.; Nakamura, T.; Itoh, M. Dielectric properties of A-site deficient perovskite-type lanthanum-calcium-titanium oxide solid solution system $[(1 - x)La_{2/3}TiO_{3-x}CaTiO_3$ $(0.1 \leq x \leq 0.96)]$. *Mater. Res. Bull.* **1995**, *30*, 307–316. [CrossRef]
26. Chung, S.Y.; Lee, S.I.; Choi, J.H.; Choi, S.Y. Initial cation stoichiometry and current-voltage behavior in Sc-doped calcium copper titanate. *Appl. Phys. Lett.* **2006**, *89*, 191907. [CrossRef]
27. Li, J.; Subramanian, M.A.; Rosenfeld, H.D.; Jones, C.Y.; Toby, B.H.; Sleight, A.W. Clues to the Giant Dielectric Constant of $CaCu_3Ti_4O_{12}$ in the Defect Structure of $SrCu_3Ti_4O_{12}$. *Chem. Mater.* **2004**, *16*, 5223–5225. [CrossRef]
28. Li, W.; Schwartz, R.W.; Chen, A.P.; Zhu, J.S. Dielectric response of Sr doped $CaCu_3Ti_4O_{12}$ ceramics. *Appl. Phys. Lett.* **2007**, *90*, 112901. [CrossRef]